

## Support information

### Oil droplets and bubbles manipulation underwater on superhydrophobic surfaces with switchable adhesion

Dejun Gao,<sup>ac</sup> Jian Cao, <sup>\*a</sup> Zhiguang Guo<sup>\*bc</sup>

<sup>a</sup> State Key Laboratory of Advanced Welding and Joining, Harbin Institute of Technology, Harbin 150001, China.

<sup>b</sup> Hubei Collaborative Innovation Centre for Advanced Organic Chemical Materials and Ministry of Education Key Laboratory for the Green Preparation and Application of Functional Materials, Hubei University, Wuhan 430062, China.

<sup>c</sup> State Key Laboratory of Solid Lubrication, Lanzhou Institute of Chemical Physics, Chinese Academy of Sciences, Lanzhou 730000, China.

*\*Corresponding author.*

Tel: 0086-931-4968105; Fax: 0086-931-8277088. Email address: [zguo@licp.cas.cn](mailto:zguo@licp.cas.cn) (Guo), Email address: [cao\\_jian@hit.edu.cn](mailto:cao_jian@hit.edu.cn) (Cao)

#### Switchable wettability strategy:

For UV light irradiation, the ablated surface was placed exactly under the UV lamp at a distance about 12cm. An 8W UV lamp with a wavelength of 253nm was used as the light source for 8h irradiation. The dark storage is realized by placing samples in a totally dark box at a room temperature for a week.

#### Characterization:

The contact angles and sliding angles were measured on a contact angle system (JC2001, Zhongchen digital equipment Co., Ltd. Shanghai, China). The volumes of water, oil droplet, bubble were 5  $\mu$ l, 10  $\mu$ l and 5  $\mu$ l respectively. 1, 2-dichloroethane and dichloromethane were used as the test oils. The morphology of surfaces and the chemical elements were studied by a scanning electron microscope (SEM, Helios Nanolab600i, FEI, USA) equipped with an energy dispersive spectrometer (EDS). The surface chemical state was analyzed by X-ray photoelectron spectroscopy (XPS, Thermo Scientific ESCALAB 250Xi). The crystalline structure and the phase analysis were detected by X-ray diffraction (XRD, D8-ADVANCE, Bruker AXS, GER) with Cu-K $\alpha$  radiation. All the optical photographs were obtained by a digital camera (Sony DSCHX200).

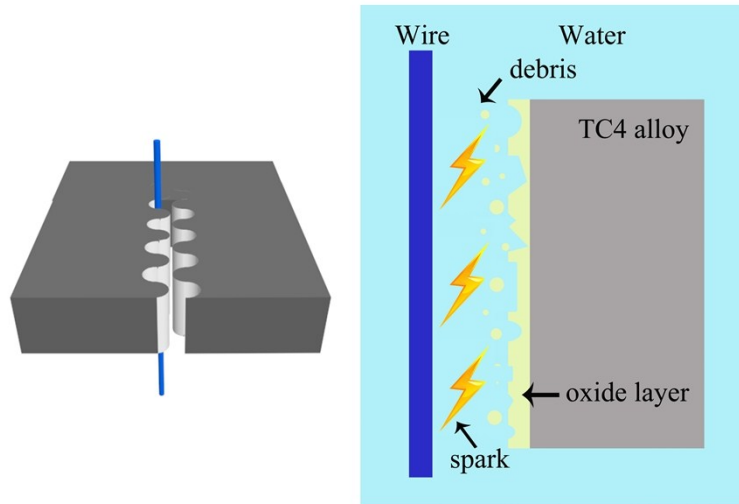


Fig. S1 Schematic diagrams of WEDM process.

By utilizing a metal wire as an electrode, an AC pulse voltage was applied between the wire and alloy. The wire didn't contact closely with alloy and there was a relatively narrow distance between them. Since the existence of a machining gap, electrical discharges were initiated and the alloy was ablated. At the same time, the quantity of heat that the electrical discharges produced led to the melting and evaporation of alloy. A large amount of randomly distributed craters and debris appeared on the alloy surface. As a medium of discharge sparks, the wire cutting fluid flowed continually to remove debris and heat. The temperature fell rapidly with the fluxion of the wire cutting fluid. The molten metal solidified quickly as a result. The alloy was ablated disproportionately and a rough metallic surface was obtained. Since the instantaneous high temperature existed, the alloy reacted with the oxygen in the air or fluid. Although wire cutting fluid was used the dielectric fluid in the machining process, the alloy was still oxidized incompletely on the surface. After this process, a hierarchical rough structure and oxides were both obtained on the ablated surface.

To further discuss the effect of different parameters on the morphology and wettability of TC4 surface, cutting speed was changed. As shown in Fig. S2, with the increase of cutting speed, the wavelength of macroscopic wavy patterns heightened, but the micro morphologies were similar. All the obtained surfaces showed excellent superhydrophobicity and were unaffected by cutting speed as shown in Fig. S3. Then the material compositions of surfaces were analysed by XRD. The results are exhibited in Fig. S4. According to the results, the phase of surfaces didn't depend on cutting speed.

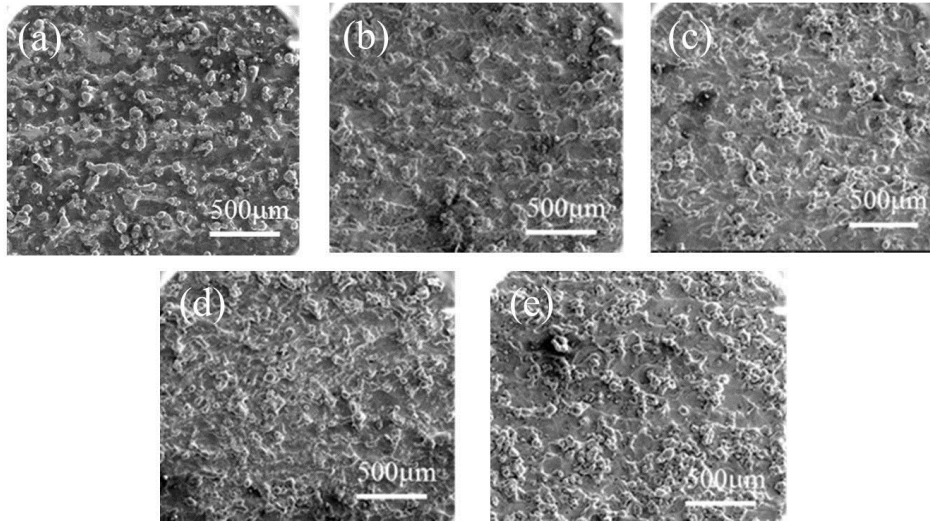


Fig. S2 SEM images of the ablated surfaces with various cutting speeds: (a) 1 mm/min (b) 2 mm/min (c) 3 mm/min (d) 4 mm/min (e) 5 mm/min

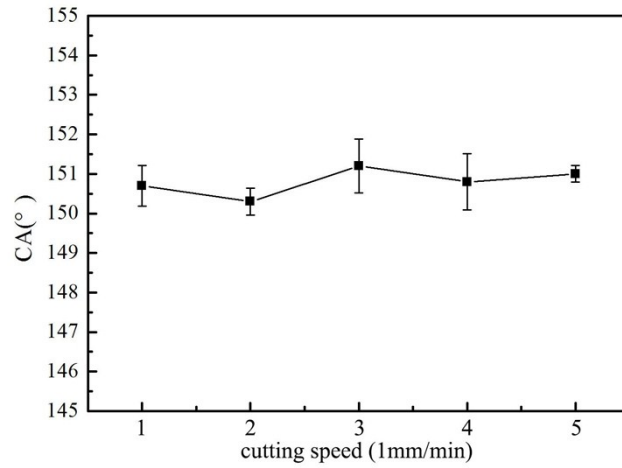


Fig. S3 The CAs of ablated surfaces with various cutting speeds.

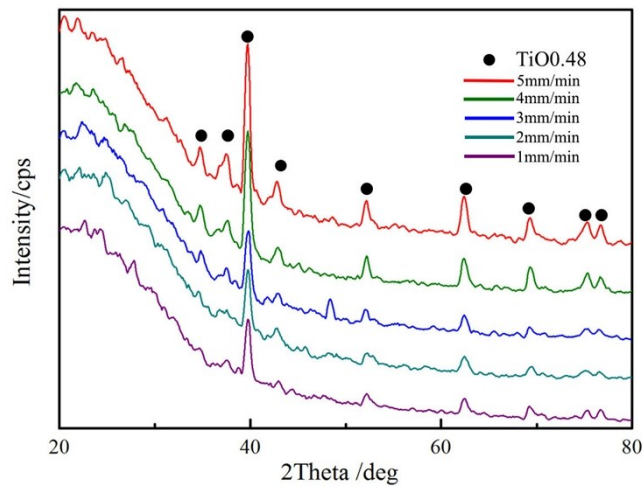


Fig. S4 The XRD results of ablated surfaces with various cutting speeds

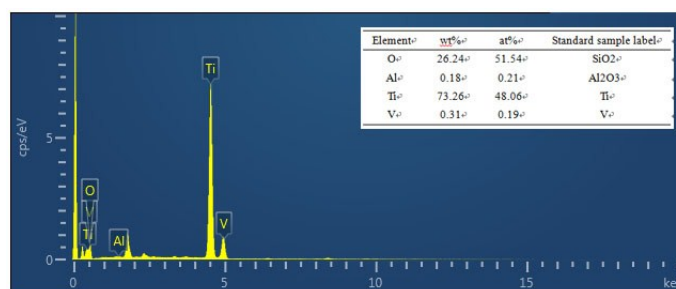


Fig. S5 EDS spectra mapping of the ablated surface

Table S1 EDS chemical analysis (at %) of different spots in Fig. 2(a)

Spot	A	B	C	D	E
Ti	54.81	72.10	63.09	48.93	30.55
O	45.19	27.90	36.91	51.07	69.45



Fig. S6 Optical image of TC4 alloy and the WCA result

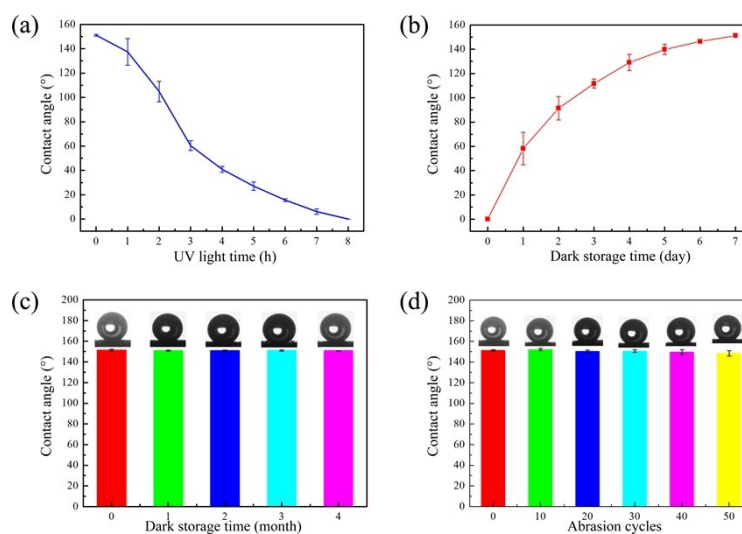


Fig. S7 (a-b) The evolution of WCA on the ablated surface under UV light irradiation and dark storage. (c) The effect of storage time on WCA. (d) The effect of abrasion cycles on WCA.

When the UV light irradiation time increases to 8h, the WCA gradually decreases from 151.2° to 0°, indicating Ti-OH groups gradually are adsorbed and the surface shows superhydrophilicity finally. With the dark storage time increasing, the WCA gradually recovers from 0° to 151° and the course is opposite to UV light irradiation. The mechanism has been illuminated above and this process can be repeated for many times. The short service life of other superhydrophobic surfaces restricts their practical applications on account of their instability. The stability of the ablated surface was tested in our paper and the result is showed in Fig. S7c. The WCA remains little change during four months without special protection. Its excellent stability benefits from no

chemical modification. After the process, the ablated surface shows superhydrophobicity without any modification. It is not only friendly to environment and innocuous to users, but also shows more stable superhydrophobicity. It means the ablated surfaces have a long service life. This can't be realized by the modified surface on account of unstable chemical modification. As far as know, the mechanical durability is still significant for the application of superwetting surfaces. To test mechanical durability, an abrasion resistance test was implemented as Fig.S8. In every cycle of abrasion, the surface was dragged for 10cm under the loading of 200g weight on the 800# sandpaper. During the abrasion test, the change of WCA is fluctuant, even appears augment in Fig. S7d. It is possible that new rough microstructure forms on account of abrasion. After 50 times abrasion, the surface still shows excellent superhydrophobicity and the SEM image of the abraded surface is showed in Fig.S9. Although some particles are damaged and debris remains on the surface, the original morphology still exists. It demonstrated that the metallurgical bonding of the oxide layer and alloy is strong. The ablated surface exhibits well mechanical durability.

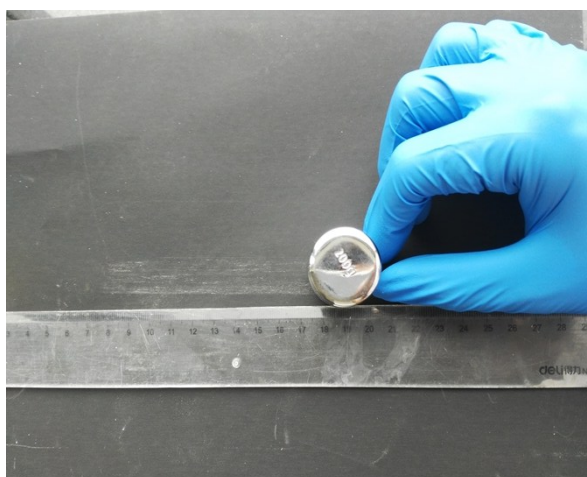


Fig. S8 Optical image of the abrasion test on 800# sandpaper at 200 g loading

The samples were cut into sheets ( $10 \times 10 \times 1$  mm<sup>3</sup>) by wire electrical discharge machining. The area of abraded surface was 100 mm<sup>2</sup>. The quality of loading was 200g and the intensity of pressure was  $1.96 \times 10^4$  Pa.

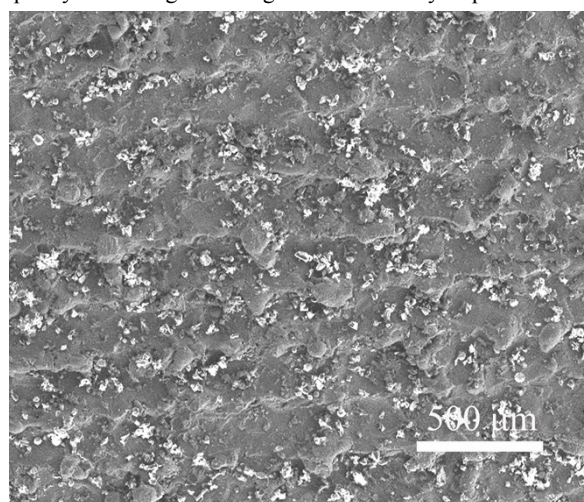


Fig. S9 SEM image of the ablated surface after abrasion test

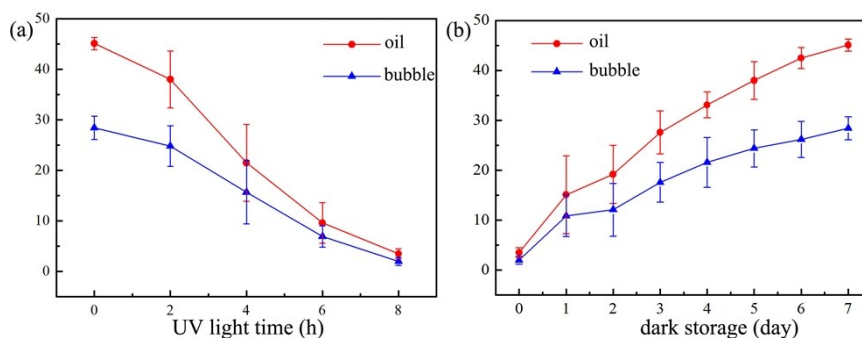


Fig. S10 The evolution of OSA and BSA on the ablated surface (a) under UV light irradiation and (b) dark storage.

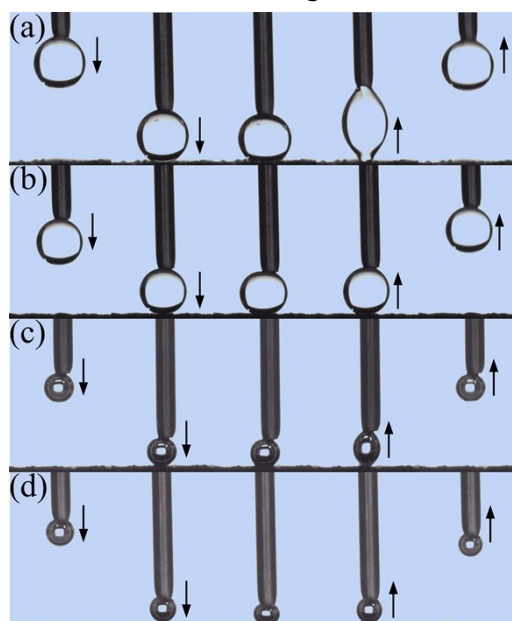


Fig. S11 (a) Dynamic underwater oil adhesion of the surface after dark storage. (b) Dynamic underwater oil adhesion of the surface after UV irradiation. (c) Dynamic underwater bubbles adhesion of the surface after dark storage. (d) Dynamic underwater bubbles adhesion of the surface after UV irradiation.

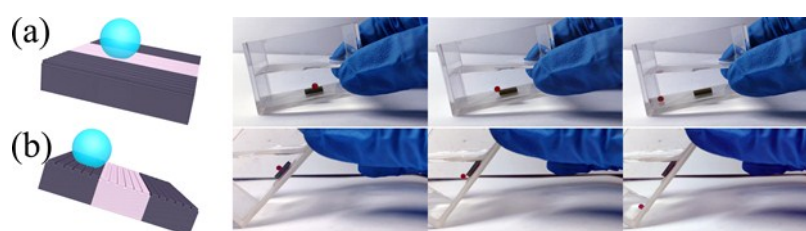


Fig. S12 (a) Oil droplet motion along the designed track. (b) Oil droplet motion out the designed track. The directional transportation of oil under water is realized by the combination of low and high adhesive surface. As mentioned above, the ablated surface is high adhesive for oil under water and becomes low adhesive after irradiation. So only the middle part was irradiated and the other part was covered to avoid UV light irradiation as shown in Fig. S12a. As a result, the middle part is low adhesive, but the other part is high adhesive for oil under water. When the surface was placed aslant and the slant angle was nearly  $5^\circ$ , an oil droplet dropped on the middle part and can roll along the irradiated part under the assistance of gravity in Fig. S12a. But when an oil droplet dropped or motioned on other part, it was adsorbed and couldn't go on roll off under this slant angle as Fig. S12b shown. The oil droplet is sessile on the surface on account of the mixed state.

The oil droplet only can move on a high slant angle. The slant angle can reach up to  $48.2^\circ$ . It demonstrates oil droplets only transported along the designed track and the directional transportation of oil under water is realized with controllable adhesion.